

## *Retraction*

# **Retracted: Application of High-Resolution Face Recognition and EDF Image Reconstruction in English Classroom Teaching**

## **Security and Communication Networks**

Received 5 December 2023; Accepted 5 December 2023; Published 6 December 2023

Copyright © 2023 Security and Communication Networks. This is an open access article distributed under the Creative Commons Attribution License, which permits unrestricted use, distribution, and reproduction in any medium, provided the original work is properly cited.

This article has been retracted by Hindawi, as publisher, following an investigation undertaken by the publisher [1]. This investigation has uncovered evidence of systematic manipulation of the publication and peer-review process. We cannot, therefore, vouch for the reliability or integrity of this article.

Please note that this notice is intended solely to alert readers that the peer-review process of this article has been compromised.

Wiley and Hindawi regret that the usual quality checks did not identify these issues before publication and have since put additional measures in place to safeguard research integrity.

We wish to credit our Research Integrity and Research Publishing teams and anonymous and named external researchers and research integrity experts for contributing to this investigation.

The corresponding author, as the representative of all authors, has been given the opportunity to register their agreement or disagreement to this retraction. We have kept a record of any response received.

## **References**

- [1] S. He and W. Zhang, "Application of High-Resolution Face Recognition and EDF Image Reconstruction in English Classroom Teaching," *Security and Communication Networks*, vol. 2022, Article ID 5877689, 10 pages, 2022.

## Research Article

# Application of High-Resolution Face Recognition and EDF Image Reconstruction in English Classroom Teaching

Shaofang He <sup>1</sup> and Wenjuan Zhang <sup>2</sup>

<sup>1</sup>International Exchange Department, Inner Mongolia Business and Trade Vocational College, Hohhot, Inner Mongolia 010010, China

<sup>2</sup>International Education Department, Inner Mongolia Business & Trade Vocational College, Hohhot, Inner Mongolia 010070, China

Correspondence should be addressed to Shaofang He; [hfh00010@163.com](mailto:hfh00010@163.com)

Received 5 May 2022; Revised 23 May 2022; Accepted 28 May 2022; Published 14 June 2022

Academic Editor: Muhammad Arif

Copyright © 2022 Shaofang He and Wenjuan Zhang. This is an open access article distributed under the Creative Commons Attribution License, which permits unrestricted use, distribution, and reproduction in any medium, provided the original work is properly cited.

This study examines classroom monitoring in order to increase the effectiveness of English classroom instruction. This article uses high-resolution algorithms and EDF image reconstruction technology in the English classroom education system to improve the high resolution of students' faces. This work presents a fast pixel capture function to enhance the rapid video capture function. The stack velocity picking of the speed spectrum is the most important aspect of velocity analysis. To create successful changes to the algorithm, this method often employs optimization algorithms as a way of stack velocity choosing speed. Finally, based on algorithm improvements, this study builds the system structure and develops simulation tests to validate system performance. The English classroom teaching system created in this work can properly determine the real-time status of students by facial recognition and has excellent user satisfaction, indicating that it may effectively increase the teaching impact, according to experimental research.

## 1. Introduction

In English classroom teaching, only using camera equipment to recognize students' faces will have obvious resolution problems. Therefore, it is necessary to improve the resolution of face recognition with the support of existing equipment.

Depth of field is the difference between the farthest clear imaging object distance and the closest clear imaging object distance of the optical system. The extended depth of field (EDF) technology has thus been developed. This technology usually refers to the use of software algorithms to solve the physical performance limitations of the optical system with a small depth of field, and it realizes the expansion of the depth of field by collecting a series of images of the same object with different focal lengths. As a relatively new technology, the depth of field expansion is still in continuous development [1].

At this stage, the conditions for the development of multiviewpoint video, from the acceptance of stereoscopic videos by users to the popularization of stereoscopic display devices, have become mature. The current main problem is the lack of multiviewpoint data sources. For multiviewpoint data acquisition, the key issue is how to effectively describe the scene and realize the effective sampling and reconstruction of the scene [2].

Through the spectrum analysis of the light field, the plenoptic sampling theory shows that the minimum sampling rate of the scene is only related to the minimum and maximum depth of the scene and has nothing to do with the depth and complexity of the scene. Because it only considered ideal scenes in the research but did not consider the existence of occlusion and non-Lambertian reflections in the scene, the corresponding research was too ideal. On this basis, the research in this paper extends the theory of all-optical sampling, analyzes non-Lambertian reflection

scenes, occluded scenes and oblique plane scenes, and obtains a more accurate minimum sampling rate and the corresponding optimal reconstruction filter [3].

Digital technology has been employed to variable degrees in numerous sectors as current computer technology advances, and digital microscopes have arisen. Video microscope is another name for the digital microscope. It uses a photosensitive sensor to gather and digitize the physical picture seen through a typical optical microscope and then sends it to a computer for display and processing. On the one hand, the digital microscope displays the picture on an easy-to-view monitor, increasing work productivity; on the other hand, the computer may do processing on the gathered original image, such as noise reduction, conversion, and synthesis, which the conventional microscope cannot see. As a result, ultra-depth-of-field microscopes are also a possibility. It may overcome the constraints of standard optical microscopes to get super-depth-of-field pictures and construct a super-depth-of-field digital microscope by using the depth-of-field image synthesis algorithm to synthesize the original imaging data given by the microscope. The ultra-depth-of-field microscope, which breaks through the depth-of-field limitation of traditional optical microscopes, plays an important role in many fields. In the research and application of biology and medicine, it is often necessary to obtain the three-dimensional structure information of the sample. When the sample is slightly larger, the traditional optical microscope cannot meet the requirements of single clear imaging.

The existing methods for extending the depth of field can be divided into two categories: nonimage synthesis-based extension methods and image synthesis-based extension methods. Among them, nonimage synthesis-based methods mainly use optical imaging principles to modify traditional microscopes, such as designing annular apertures and reducing apertures, but such methods cannot break through the limit of the depth of field, nor can they design superdepth microscopes. The method based on image synthesis is to obtain a globally clear all-focus image by fusing the locally focused image sequence according to certain rules. In theory, this kind of method can infinitely expand the depth of field and design a superdepth microscope. Regarding the image fusion algorithm, three categories can be summarized according to the stage of the image fusion process: pixel-level fusion, feature-level fusion, and decision-level fusion.

Based on the above analysis, this paper applies EDF image reconstruction technology to English classroom teaching to build a new intelligent high-resolution face recognition system, which monitors the status of students in real time and improves the effectiveness of English classroom teaching.

## 2. Related Work

Image fusion methods based on the spatial domain mainly integrate image pixels by directly analyzing the spatial characteristics of the original image pixels. This type of method is the most intuitive and the fastest method.

In the image fusion method based on spatial domain, the original image is often required to be divided into blocks. The literature [4] proposed a block-based image fusion method. This method first divides the original image into fixed-size image blocks, then compares the spatial frequency in each space block to obtain the fusion result of the corresponding position according to certain rules, and finally obtains the fusion image. However, this method has an obvious disadvantage; that is, it is prone to block effects. Too large a block can easily cause pixels of different definitions to be divided into the same block, while a block that is too small often cannot reflect the characteristics of the block. On the other hand, the degree of focus of image subblocks is difficult to measure. Literature [5] improved the image fusion method and used an artificial neural network to classify the features of the image block, so as to judge the fast focus attribute of the image. It is not difficult to see that the main aspects that affect performance in this type of method are the following two points. One is the block method and rule of the original image, and the second is the quantitative calculation of the focus attribute of the image block, which is the feature calculation method. The excellence of these two aspects directly affects the quality of the fusion result. In view of the two problems of this block fusion algorithm, scholars have made a series of improvements to it. The literature [6] proposed a fusion method based on local focus estimation. This method gets rid of the rectangular limitation of traditional block segmentation and segments the original image in a nonrectangular form according to the distribution of the focus position, which alleviates the block effect to a certain extent. The literature [7] evaluated several commonly used focus measurement methods, including image variance, gradient energy, and spatial frequency. The literature [8] used a genetic algorithm to optimize the method of the image block. The literature [9] used a differential evolution algorithm to optimally solve the block size. The literature [10] used a quadtree to adaptively block the original image and greatly improves the effect of image fusion through the adaptive block rule.

The Bayesian model optimization method's goal is to find a solution that maximizes the prior probability, which is the fused picture we are looking for. To achieve sensor image fusion, the literature [11] employed a simple adaptive algorithm to evaluate the features of the acquired sensor and the link between distinct sensors. A probabilistic image fusion approach based on an image information model was developed in the literature [12]. The Markov random field method involves converting the fusion process into a suitable cost function that may successfully correlate to the fusion outcome image. A Markov fusion model based on the similarity of matched pictures was presented in the literature [13]. In the literature [14], a Markov random field is presented that solely addresses the picture's edge structure and is utilized in conjunction with iterative conditions to accomplish the goal of image fusion. The literature [15] offered an exchange iteration approach for improving texture and terrain estimation, which produced excellent results.

The literature [16] proposed an image fusion method based on Ridgelet to improve the image fusion effect to a

certain extent. The literature [17] proposed an image fusion method based on contourlet transform contourlet, which compares the maximum area energy to select high-frequency subband coefficients to improve the fusion quality. The literature [18] proposed a Bandelet-based image fusion method, which uses the maximum principle to select transform coefficients and also obtains a good fusion effect. The literature [19] proposed a method based on the Log-Gabor transform. The literature [20] proposed an image fusion method based on contourlet packet transform.

### 3. EDF Image Reconstruction Algorithm

The key point of velocity analysis is the velocity spectrum stack velocity picking velocity. This process usually uses optimization algorithms as the means of stack velocity picking velocity. Here, we first introduce the first intelligent search for optimal solution technology-nonlinear function method. The nonlinear function method established in this paper is used as a constraint condition. The search path of the target area is set by the nonlinear function, the appropriate window is selected, and the velocity spectrum energy cluster extreme value is searched along the path. The picking process takes the nonlinear function as the nonlinear constraint function, and its general expression is

$$f(x) = a_0x^n + a_1x^{n-1} + \dots + a_{n-1}x + a_n. \quad (1)$$

Among them,  $a_0 \neq 0, a_i (i = 0, 1, \dots, n)$  is a real number.

This function is also called  $n$ -th order algebraic equation in mathematics and has  $n$  roots. Since the function is always in the process of intelligently searching for the optimal solution, there is always at least a quadratic term in  $x$ , so the function is always nonlinear. The basic relationship established between this function and the velocity spectrum is as follows: three approximate roots  $x_k, x_{k-1}, x_{k-2}$  as nodes are equivalent to several large energy cluster points selected on the velocity spectrum, and the appropriate parabolic path is selected to be searched out as the required root  $x^*$ , that is, the stacking velocity. The solution process of this function is graphically represented in Figure 1 [21].

The interpolation polynomial is as follows:

$$y(x) = f(x_k) + f(x_k, x_{k-1})(x - x_k) + f(x_k, x_{k-1}, x_{k-2})(x - x_k)(x - x_{k-1}) + \dots \quad (2)$$

Two zero points are obtained:

$$x_{k+1} = x_k - \frac{2f(x_k)}{\omega \pm \sqrt{\omega^2 - 4f(x_k)f(x_k, x_{k-1}, x_{k-2})}}. \quad (3)$$

Among them,

$$\omega = f(x_k, x_{k-1}) + f(x_k, x_{k-1}, x_{k-2})(x - x_{k-1}). \quad (4)$$

The above is a simple interpolation calculation method.

The three variables  $x_k, x_{k-1}, x_{k-2}$  in the above formula can also be called three nodes. How to obtain these three variables is the key to realizing the programming of the nonlinear function method. We first assume that  $x_k$  is closer

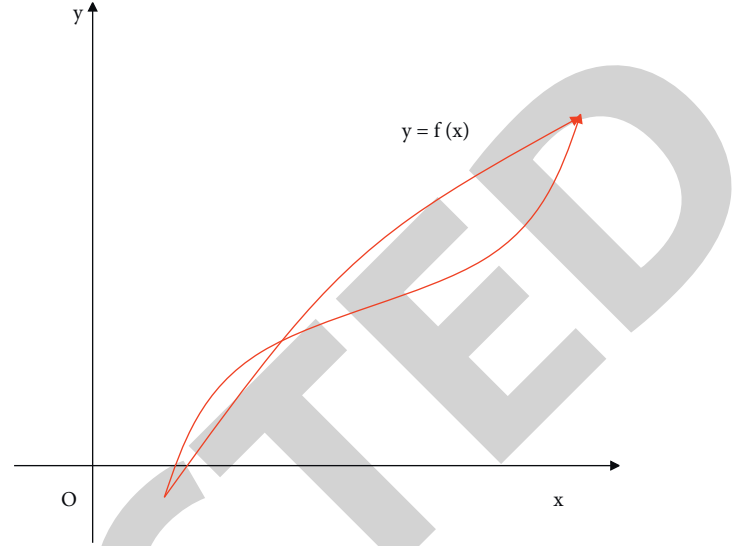


FIGURE 1: Schematic diagram of nonlinear function solution.

to the next node  $x^*$ . At this time, we choose  $x_k$ , which is closer to  $x_{k+1}$ , as the new approximate solution. The whole procedure of solving all solutions may be accomplished via analogy. However, the nonlinear function approach's procedure of intelligently looking for the best solution in the velocity spectrum differs from the conventional way of solving nonlinear functions. The coefficient value and  $y$  value of each  $x$  term are known in the classic method of solving nonlinear functions, and  $x$  is solved. However, in the velocity spectrum application procedure,  $x$  is the velocity spectrum's unique horizontal or vertical coordinate, which is a known number. The coefficient  $a$  controls the direction of the picking path and is set in advance during the programming process. However,  $y$  is an unknown quantity, that is, the optimal solution to be searched. The specific process is as follows [22].

The velocity spectrum not only reflects the reflected wave energy of each CMP gather but also reflects the wave impedance of the underground interface. It is approximately regarded as a two-dimensional numerical matrix. The zero-offset time  $t_0$  and superimposed velocity  $v$  in the velocity spectrum are represented by row  $i$  and column  $j$  of the two-dimensional numerical matrix, respectively. Moreover, each two-dimensional coordinate determines a node  $\text{sem}(i, j)$ , which represents the velocity energy value. The magnitude of this value is the standard of the picking speed, and the picking process can be transformed into a search of a two-dimensional numerical matrix. Since the distribution of velocity spectrum energy clusters can be found regularly, the established pick-up path of the nonlinear function can be saved in the form of discrete points. When  $n = 2$ , the above formula becomes

$$j = A * i^2 + B * i + C. \quad (5)$$

The search path of the nonlinear function method in the velocity spectrum is determined by  $A, B$ , and  $C$  together. As shown in Figure 2, according to the distribution law of the

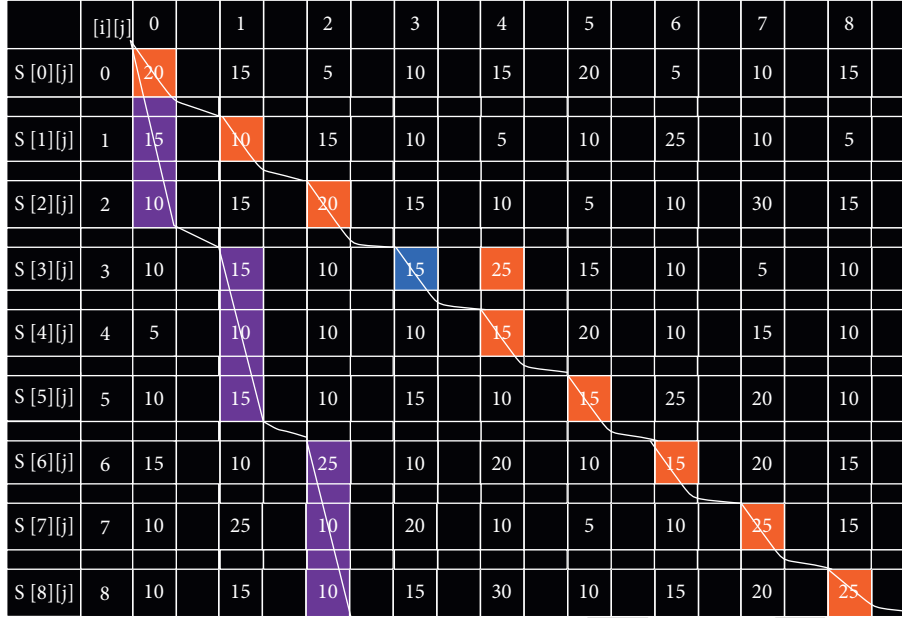


FIGURE 2: Schematic diagram of search paths for different coefficients.

velocity spectrum energy cluster, a two-dimensional velocity spectrum value matrix with  $8 \times 8$  columns is constructed. The green box picking path coefficient in Figure 2 is  $A = 1/100, B = 1/3, C = 0$ , and the blue box picking path coefficient is  $A = 1/100, B = 1, C = 0$ . It can be clearly seen that there are obvious differences in the results of the two path searches.

It can be seen from Figure 2 that this form is not an ideal energy value, and the optimal energy value at this moment is adjacent to the yellow box. We determine the search bandwidth by opening a window to the left, right, or both sides based on the picking path. Due to the limited scope of the chart, the purple box is the path determined by the nonlinear function method set by  $A = 1/100, B = 1/3, C = 0$ , and the red box is the path determined by the nonlinear equation method set by  $A = 1/100, B = 1/4, C = 4$ . After that, we use the respective windows as the baseline to extend 1 and 2 points to the right, as shown in Figure 3.

From Figure 3, we can see that it is not the origin of the coordinates as the starting point. This is an artificially given initial speed; that is, given a value of  $C$ , the initial point position is the default in the program, although the nonlinear function method is for the initial speed. There is no strong dependence, but for the velocity spectrum of the low-velocity layer, too much local extreme point interference can be avoided by setting the initial velocity. We have also seen that based on the determination of the two search paths, the set left and right limit windows make the search range subject to certain constraints, but it is more accurate than picking only points on the path determined by the nonlinear function. As for how large the time window is, it depends on the actual range of the velocity spectrum. The window used in this article is 21. If the range of the window is the entire velocity spectrum, then only  $A$  slope is sufficient, but the entire velocity spectrum search will be interfered with by

many high-energy clusters on the surface and the boundary. At the same time, compare the path with the largest energy cluster on the path among more than a dozen paths set in the program, and save all the energy values on this search path, which is the superimposition speed we want to keep.

The Viterbi method is a branch of probability theory known as Markov theory. It is also known as the shortest route search algorithm. In the sphere of electronic communications, the Viterbi algorithm was initially used. The theoretical framework is now pretty established after decades of research. It is as follows. There are various transmission channels between the beginning state sequence and the end state sequence, and under the constraint of a given discriminant function, the most satisfactory discriminant function is sought. The specific process is as follows.

The discrete points in the target area are set to a known state sequence:

$$S = s_1^T (s_1, s_2, \dots, s_T). \quad (6)$$

If it is assumed that the state  $s_t$  at time  $t$  occurred in the state before  $s_{t-1}$ , then the relationship between the two is

$$P(s_1^T) = P(s_1) \prod_{t=2}^T P(s_t | s_1^{t-1}). \quad (7)$$

In the formula,  $P(s_t | s_1^{t-1})$  is the posterior probability of the required probability  $P(s_1^T)$ , and  $P(s_1)$  is the prior probability of the required probability  $P(s_1^T)$ . In order to maximize the value of the probability  $P(s_1^T)$ , the various transmission paths mentioned before are set as the transmission sequence.

$$G = g_1^T (g_1, g_2, \dots, g_T). \quad (8)$$

Then, the relationship between the transferred value  $g_t$  at time  $k$  and  $g_{t-1}$  can also be expressed as

	[i][j]	0	1	2	3	4	5	6	7	8
S[0][j]	0	20	15	5	10	15	20	5	10	15
S[1][j]	1	10	10	15	10	5	10	25	10	5
S[2][j]	2	5	25	15	20	15	5	10	30	15
S[3][j]	3	25	10	5	15	25	15	10	5	10
S[4][j]	4	5	15	10	10	15	20	10	15	10
S[5][j]	5	10	5	10	15	10	15	15	20	10
S[6][j]	6	15	10	25	10	20	10	15	20	15
S[7][j]	7	10	30	10	20	10	5	10	25	15
S[8][j]	8	10	15	10	15	30	10	15	20	25

FIGURE 3: Schematic diagram of the path after adding a window.

$$P(g_1^{T-1}) = P(g_1) \prod_{t=2}^{T-1} P(g_t | g_1^{t-1}). \quad (9)$$

Since  $G$  is the intermediate transfer sequence of  $S$ , the following relationship can be established between the two:

$$\begin{cases} P(s_t | g_1^t, s_1^{t-1}) = P(s_t | g_t), \\ P(g_{t+1} | g_1^t, s_1^{t-1}) = P(g_{t+1} | g_t), \end{cases} \quad (10)$$

Through further derivation, we have

$$P(s_1^T, g_1^T) = P(g_1) \prod_{t=2}^{T-1} P(g_t | g_1^{t-1}) \prod_{t=2}^{T-1} P(s_t | g_t). \quad (11)$$

It can be concluded from the above formula that the forward calculation of all state sequences and transfer sequences in the target area has been completed. The reverse tracking process of the maximum probability  $P(g_1^{T-1})$  inferred from the current state sequence  $s_1^T$  can be obtained by the following formula:

$$\max g_1^{T-1} = \max | g_1^T P(g_1^T | s_1^T). \quad (12)$$

According to the shortest path principle of the Viterbi algorithm and the above, a two-dimensional array  $V(i, t)$  is introduced, and the above-mentioned forward calculation and reverse tracking problems can be expressed as

$$V(i, t) = \max | g_1^T P(s_1^T, g_1^T, g_t = i). \quad (13)$$

From this recursion, we can obtain

$$V(i, t) = P(s_1^T | g_t = i) \max | g_1^T P(s_1^T, g_1^T, g_t = i) V(i, t-1). \quad (14)$$

The above is the basic derivation process of the Viterbi algorithm.

Similar to the numerical simulation process of the nonlinear function method, the Viterbi algorithm is introduced into the process of automatically picking up the superimposed velocity. First, the velocity spectrum needs to be regarded as a two-dimensional numerical matrix, and the zero-offset time  $t_0$  and the stacking velocity  $v$  are represented by row  $i$  and column  $j$  of the two-dimensional array, respectively. Moreover, all the velocity energy values  $\text{sem}(i^T, j^T)$  in the velocity spectrum are regarded as the initial state sequence:

$$S = s_1^T (s_1, s_2, \dots, s_T). \quad (15)$$

The final state sequence obtained by the forward calculation of the Viterbi algorithm is set to  $\text{sem}'(i^T, j^T)$ , that is,  $S'$ . After that, the maximum state value in the final state sequence is found, and it is traced backward through the transfer sequence

$$G = g_1^T (g_1, g_2, \dots, g_T), \quad (16)$$

related to the maximum state value. This tracking path is the desired result.

According to the distribution law of the velocity spectrum energy clusters, a two-dimensional velocity spectrum numerical matrix with  $9 \times 9$  columns is constructed. The specific application of the Viterbi algorithm is shown in Figure 4, and the window is 3.

It can be seen from Figure 4 that the initial state sequence  $S[0][j]$  is integrated along the longitudinal direction. As  $i$  increases,  $S'[i][j]$  changes continuously, and  $S'[i][j]$  is the sum of the maximum of the three values of  $S[i][j]$  at time  $i$  and  $S[i-1][j-1]$  and  $S[i-1][j+1]$  at time  $i-1$ . This process is called the forward calculation of the Viterbi algorithm. At the last moment  $i = 9$ , the final state  $S'[9][9] = 225$  is the maximum value of the entire region. Since the transfer sequence  $G[i][j]$

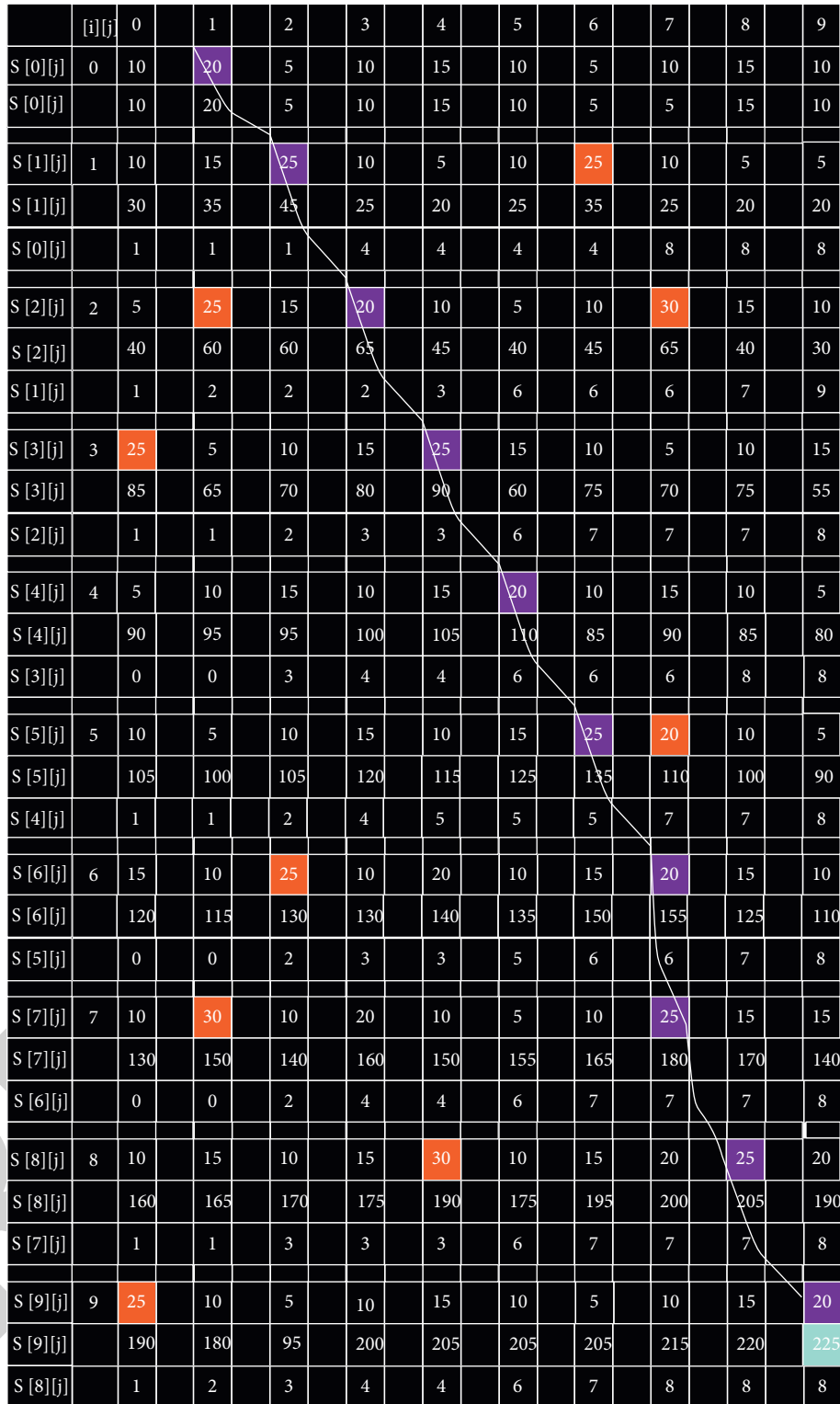


FIGURE 4: Schematic diagram of the numerical simulation calculation of the Viterbi algorithm.

records the coordinates of the previous state related to this state,  $G[0][2]$  can be found step by step by the transfer sequence  $G[8][9]$ . This process is called the reverse tracking of the Viterbi algorithm. The green box in Figure 4 is the result of the final search, and the blue box in Figure 4

represents the larger value of the initial state at that moment. Although the value is large, it is not the final desired result, that is, the interference value. These values are removed by the reverse tracking of the final maximum value.

### 4. English Classroom Teaching System Based on High Resolution and EDF Image Reconstruction

This article introduces high-resolution and EDF image reconstruction technology to the English classroom teaching system, which can be employed in both conventional and distant English classroom teaching.

Carry out the overall system function design based on the user’s demand analysis. Teachers and students are the primary users of this system, and kids are the primary service goals of the system’s design and development. To begin, this study uses students as an example. The main interface is made of four functional modules, which include course materials, theoretical testing, communication and sharing, and personal center modules, when a student user joins the APP system via a registered account and accesses the main interface following identification verification. The overall function framework of the system is shown in Figure 5.

The auxiliary teaching APP has added a face sign-in function. The design and implementation of face check-in and attendance are mainly related to various subtype face recognition controls and check-in pictures through a face recognizer in the SDK (protection layer) to complete and judge the user’s face needs. The system supports users to recognize multiple targets, and users can sign in by traveling together. The sign-in function increases the student attendance rate, saves the time for roll call, and effectively avoids the phenomenon of students taking the sign. The realization of the face recognition sign-in function is shown in Figure 6.

The background management module mainly includes classroom management, registration management, login management, cloud disk file management, live broadcast list and content management, and personal settings and search management, as shown in Figure 7.

Chat means that after students ask questions online, teachers use text or voice to answer questions for students at fixed points, that is, use online one-to-one to simulate offline real-time answering questions. Teaching interaction means that teachers and students can communicate directly with each other in voice and text, as shown in Figure 8. When students have problems, they can ask questions in time, and then the teacher can explain. Before asking the question, the students first give the prompt on the text and click on the teacher’s avatar directly. After that, the system will provide a list of teachers who have watched the live video of the classroom, and then the user will directly select the teacher to start chatting.

### 5. System Test

Multiple integration tests are included in the idea of system testing. In order to identify potential issues that users may encounter when utilizing the English teaching system, this system’s test cases primarily consist of three aspects: client-side application testing, network-side application testing, and server-side application testing. In these three locations, tests are undertaken, and then analysis and predictions are

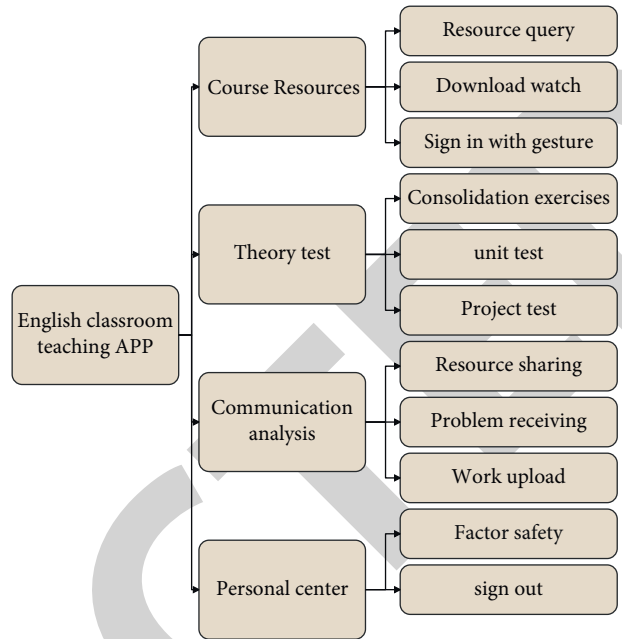


FIGURE 5: The overall function framework of the system.

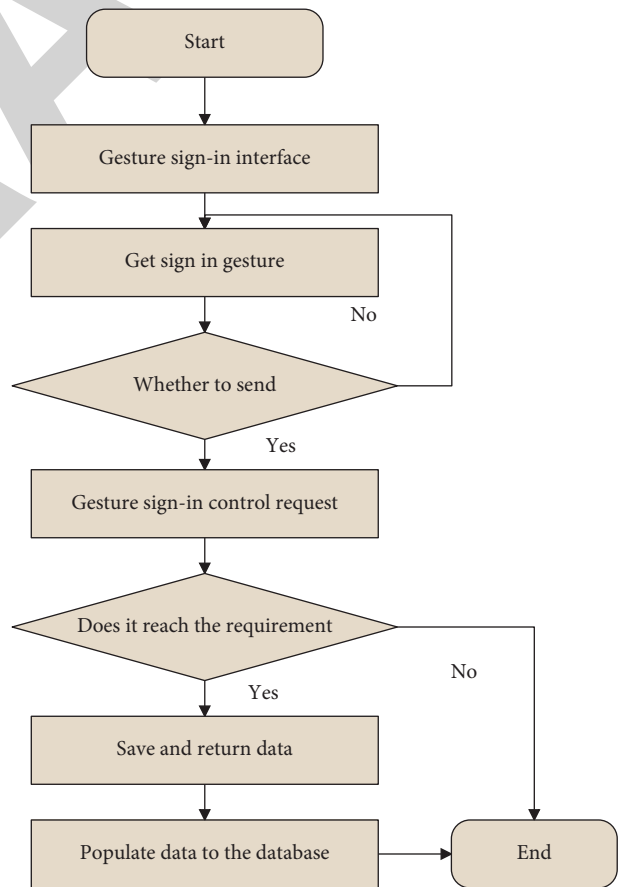


FIGURE 6: Flow chart of face recognition sign-in function.

produced. The client-side exam of the application is the most crucial of them all, and it is also the one that students need the most. At the same time, the application’s server-side



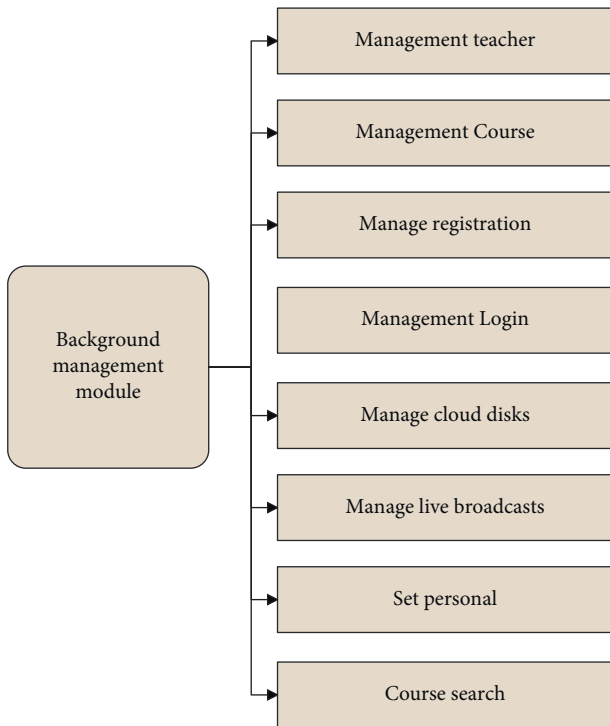


FIGURE 7: Background management module.

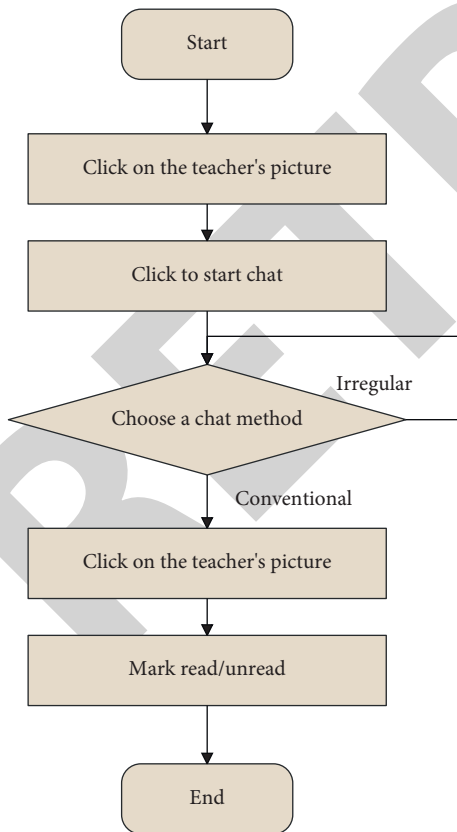


FIGURE 8: Flow chart of teaching interaction.

testing is crucial. As a result, this article combines the two, evaluating the program on the server while also testing the application on the client.

TABLE 1: Statistical table of accuracy of face state recognition of students in English class.

Number	Accuracy (%)	Number	Accuracy (%)	Number	Accuracy (%)
1	85.0	25	85.2	49	88.1
2	83.9	26	91.1	50	91.1
3	89.1	27	82.4	51	82.8
4	82.5	28	88.8	52	89.6
5	84.2	29	87.7	53	84.8
6	82.6	30	91.5	54	88.4
7	89.9	31	84.8	55	85.1
8	87.2	32	83.9	56	85.1
9	87.0	33	89.0	57	85.8
10	84.6	34	83.2	58	84.8
11	81.1	35	90.4	59	81.8
12	81.7	36	87.2	60	85.1
13	84.8	37	82.8	61	89.2
14	83.9	38	89.3	62	82.8
15	87.5	39	87.2	63	90.2
16	84.4	40	84.8	64	87.4
17	90.9	41	88.2	65	91.7
18	87.3	42	81.7	66	81.1
19	89.7	43	82.3	67	87.0
20	82.0	44	86.6	68	85.4
21	90.4	45	81.3	69	90.7
22	86.4	46	83.4	70	91.9
23	88.0	47	87.4	71	90.6
24	90.6	48	89.2	72	87.7

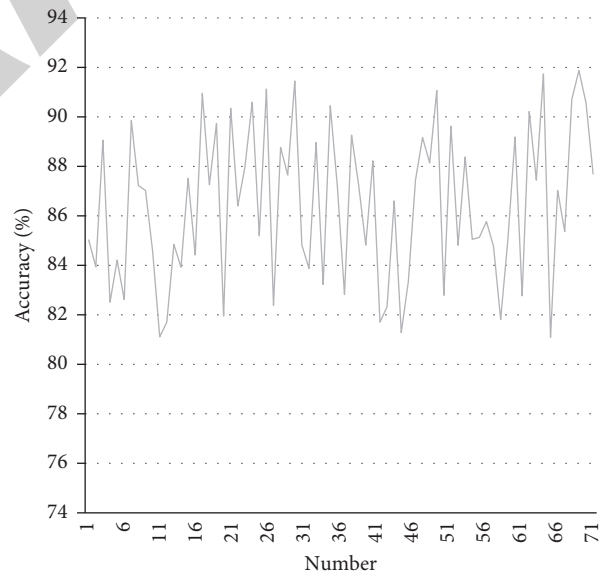


FIGURE 9: Statistical diagram of the accuracy of face state recognition of students in English class.

According to the above test requirements, this paper conducts the client-side test through setting test and combines network-side test and client-side test. This article mainly tests the user satisfaction of the English teaching system, and the server-side test is to test the accuracy of the student's state recognition, so the final test result of this paper is the student's face state recognition and user satisfaction.

TABLE 2: Statistical table of user satisfaction.

Number	Satisfaction	Number	Satisfaction	Number	Satisfaction
1	94.4	25	86.9	49	92.6
2	93.5	26	91.9	50	94.9
3	96.1	27	85.5	51	88.3
4	88.9	28	91.1	52	92.5
5	89.0	29	90.5	53	90.5
6	90.8	30	88.2	54	86.3
7	89.7	31	95.6	55	92.1
8	88.1	32	96.5	56	90.3
9	86.6	33	96.6	57	95.3
10	87.9	34	85.4	58	93.7
11	89.2	35	95.5	59	85.9
12	90.0	36	88.0	60	96.3
13	86.5	37	94.7	61	90.9
14	94.2	38	86.1	62	88.4
15	90.2	39	93.6	63	95.8
16	91.6	40	93.1	64	94.5
17	86.7	41	86.1	65	94.6
18	86.2	42	86.1	66	89.8
19	86.9	43	87.8	67	92.7
20	89.0	44	94.9	68	85.5
21	90.6	45	88.6	69	89.4
22	94.6	46	96.7	70	95.9
23	96.5	47	91.2	71	90.5
24	86.3	48	92.9	72	93.4

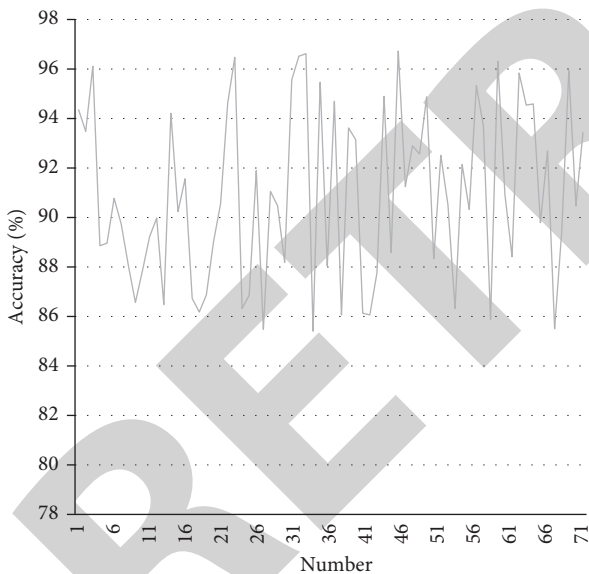


FIGURE 10: Statistical diagram of user satisfaction.

Through experimental research, the accuracy of face state recognition of students is obtained, and the results are shown in Table 1 and Figure 9.

From the above experimental research, it can be seen that the English classroom teaching system constructed in this paper can accurately identify the real-time status of the students through the face recognition of the students. On this basis, the user satisfaction is tested and the results are shown in Table 2 and Figure 10.

The above results indicate that user satisfaction is high, which further illustrates the reliability and practical effects of the system in this paper.

## 6. Conclusion

In English classroom teaching, only using camera equipment to recognize students' faces will have obvious resolution problems. Therefore, it is necessary to improve the resolution of face recognition with the support of existing equipment. This text carries on the overall functional design of the system according to the user's demand analysis. Teachers and students are the primary users of this system, and kids are the primary service goals of the system's design and development. This research combines EDF image reconstruction technology with English classroom education in order to create a new intelligent high-resolution face recognition system that monitors students' status in real time and increases English classroom teaching efficacy. This study also creates simulation tests to test system performance. The English classroom teaching system built in this study can properly determine the real-time status of students by facial recognition and has excellent user satisfaction, indicating that it may effectively increase the teaching impact, according to experimental research.

## Data Availability

The data used to support the findings of this study are available from the author upon request.

## Conflicts of Interest

The author declares that he has no conflicts of interest.

## References

- [1] M. S. Hossain and G. Muhammad, "Cloud-assisted speech and face recognition framework for health monitoring," *Mobile Networks and Applications*, vol. 20, no. 3, pp. 391–399, 2015.
- [2] A. Anjos, M. M. Chakka, and S. Marcel, "Motion," *IET Biometrics*, vol. 3, no. 3, pp. 147–158, 2014.
- [3] L. Zhuang, T. H. Chan, and A. Y. Yang, "Single-sample face recognition with image corruption and misalignment via sparse illumination transfer[J]," *IEEE Computer Society Conference on Computer Vision and Pattern Recognition*, vol. 114, no. 2-3, pp. 272–287, 2014.
- [4] G. Wang, N. Shi, Y. Shu, and D. Liu, "Embedded manifold-based kernel Fisher discriminant analysis for face recognition," *Neural Processing Letters*, vol. 43, no. 1, pp. 1–16, 2016.
- [5] T. Chuk, A. B. Chan, and J. H. Hsiao, "Understanding eye movements in face recognition using hidden Markov models," *Journal of Vision*, vol. 14, no. 11, p. 8, 2014.
- [6] H. Bouchech, "Selection of optimal narrowband multispectral images for face recognition[J]," *monthly notices of the royal astronomical society*, vol. 402, no. 4, pp. 2140–2186, 2015.
- [7] R. Ramachandra and C. Busch, "Presentation attack detection methods for face recognition systems: a comprehensive survey [J]," *ACM Computing Surveys*, vol. 50, no. 1, pp. 8.1–8.37, 2017.
- [8] Z. Huang, S. Shan, R. Wang, and H. S. Zhang, "A benchmark and comparative study of video-based face recognition on COX face database," *IEEE Transactions on Image Processing*, vol. 24, no. 12, pp. 5967–5981, 2015.

- [9] C. P. Chia-Po Wei and Y.-C. F. Wang, *IEEE Transactions on Image Processing*, vol. 24, no. 6, pp. 1722–1734, 2015.
- [10] N. L. Ajit Krishna, V. K. Deepak, K. Manikantan, and S. Ramachandran, “Face recognition using transform domain feature extraction and PSO-based feature selection,” *Applied Soft Computing*, vol. 22, pp. 141–161, 2014.
- [11] R. Weng, J. Lu, and Y.-P. Tan, “Robust point set matching for partial face recognition,” *IEEE Transactions on Image Processing*, vol. 25, no. 3, pp. 1163–1176, 2016.
- [12] Z. Cui, H. Chang, S. Shan, and B. X. Ma, “Joint sparse representation for video-based face recognition,” *Neurocomputing*, vol. 135, pp. 306–312, 2014.
- [13] P. J. Phillips and A. J. O’Toole, “Comparison of human and computer performance across face recognition experiments,” *Image and Vision Computing*, vol. 32, no. 1, pp. 74–85, 2014.
- [14] D. Tang, N. Zhu, F. Yu, and W. T. Chen, “A novel sparse representation method based on virtual samples for face recognition,” *Neural Computing & Applications*, vol. 24, no. 3–4, pp. 513–519, 2014.
- [15] R. Mehta, J. Yuan, and K. Egiazarian, “Face recognition using scale-adaptive directional and textural features,” *Pattern Recognition*, vol. 47, no. 5, pp. 1846–1858, 2014.
- [16] R. Raghavendra, K. B. Raja, and C. Busch, “Presentation attack detection for face recognition using light field camera,” *IEEE Transactions on Image Processing*, vol. 24, no. 3, pp. 1060–1075, 2015.
- [17] M. Yang, P. Zhu, F. Liu, and L. Shen, “Joint representation and pattern learning for robust face recognition,” *Neurocomputing*, vol. 168, pp. 70–80, 2015.
- [18] Y. Yan, H. Wang, and D. Suter, “Multi-subregion based correlation filter bank for robust face recognition,” *Pattern Recognition*, vol. 47, no. 11, pp. 3487–3501, 2014.
- [19] Z. Fan, M. Ni, and Q. Zhu, “Weighted sparse representation for face recognition[J],” *Neurocomputing*, vol. 151, pp. 304–309, 2015.
- [20] X. Tang, G. Feng, and J. Cai, “Weighted group sparse representation for undersampled face recognition,” *Neurocomputing*, vol. 145, pp. 402–415, 2014.
- [21] W. Hussein Al-Arashi, H. Ibrahim, and S. Azmin Suandi, “Optimizing principal component analysis performance for face recognition using genetic algorithm,” *Neurocomputing*, vol. 128, pp. 415–420, 2014.
- [22] A. Morelli Andrés, S. Padovani, M. Tepper, and J. Jacobo-Berlles, “Face recognition on partially occluded images using compressed sensing,” *Pattern Recognition Letters*, vol. 36, no. 1, pp. 235–242, 2014.